

# ACOUSTIC EMISSION CHARACTERISTICS AND FELICITY EFFECT OF WOOD FRACTURE PERPENDICULAR TO THE GRAIN

Y Wu<sup>1</sup>, ZP Shao<sup>1,\*</sup>, F Wang<sup>1</sup> & GL Tian<sup>2</sup>

<sup>1</sup>College of Forestry, Anhui Agricultural University, 130 West Changjiang Rd, 230036, Hefei, China

<sup>2</sup>International Center for Bamboo and Rattan, No. 8 Futong East Street, Wangjing Area, Chaoyang District, 100102, Beijing, China

Received June 2013

**WU Y, SHAO ZP, WANG F & TIAN GL. 2014. Acoustic emission characteristics and Felicity effect of wood fracture perpendicular to the grain.** The processes of wood fracture perpendicular to the grain of standard and notched specimens of one softwood and one hardwood were studied for the timbers' acoustic emission (AE) characteristics. The fracture evolution and mechanisms observed from their microscopic structures are discussed. AE event counts developed slowly and most were the low amplitude AE events at the low strains and a large number of high amplitude AE events appeared at the peak load or fracture stage for standard specimens. The initiation and expansion of the crack tip could be monitored efficiently by the AE technique in the three-point bending test for notched specimens. The AE signals were related to different damage modes. The AE characteristics of cell-wall fracture were high amplitude, high energy and long-duration AE events but the AE characteristics of cell-wall damage and spallation, cell-wall buckling and collapse were low amplitude, low energy and short-duration AE events. The Kaiser effect appeared at low loading and the Felicity effect at high loading under repeated wood bending loading. The Felicity ratio could better indicate the degree of damage of the wood structure.

Keywords: Wood fracture, structural damage, signal characteristics, anatomical changes

## INTRODUCTION

Acoustic emission (AE) is a widely used non-destructive technique for detecting damage evolution in various materials. It is defined as a transient elastic wave generated by the rapid release of energy within a material. It was first applied to metal fracture by Kaiser (1950) in Germany and then further developed elsewhere. Studies of wood using acoustic emission have increased over the past 30 years. Acoustic emission is mainly used in two areas. Firstly it is applied to monitor and control the drying of wood in order to eliminate or minimise drying defects (Noguchi et al. 1987, Quarles 1992, Booker 1994a,b). Secondly it has been used to monitor fracture behaviour in wood during loading.

The acoustic emission technique is sensitive to crack nucleation and growth and its special function in dynamic monitoring. It has been utilised in exploring damage and fracture mechanism and strength performance of

composite materials and made great strides. Ono et al. (1991) studied the fracture mechanism of carbon-fibre-reinforced thermoplastic composites and successfully distinguished two fracture modes, i.e. fibre breakage and delamination. They found peak amplitude, signal duration and energy distributions of AE events different in different fracture modes. Bakuckas et al. (1994) used the acoustic emission technique to locate and monitor damage growth in titanium matrix composites and correlations between the observed damage growth mechanisms; the AE results in terms of the event amplitude were established. Katsaga et al. (2007) employed acoustic emission techniques to investigate the process of fracture formation in large, shear-critical, reinforced concrete beams and to gain improved insight into the mechanisms of shear failure. They demonstrated AE techniques emerging as powerful tools in studying different aspects of the mechanisms

\*szp8@163.com

of failure in reinforced concrete. Bucur (1995) expounded the principles and gave a literature review of the AE technique of wood. He indicated that crack nucleation and growth result in a sudden change of energy within a material which thus allows acoustic emission to be used as an analytical tool for monitoring crack nucleation and growth. Schniewind et al. (1996) examined AE signals during mode I and mixed mode tests at different moisture contents and temperatures and found that the AE activity in mixed mode tests was much higher than that in mode I. Aicher et al. (2001) used AE to localise crack nucleation in glulam loaded in tension perpendicular to the grain. Dill-Langer and Aicher (2000) used the AE technique to monitor the fracture of clear spruce wood under tensile loading and found that there was an onset of AE prior to the first visible crack growth step. Reiter et al. (2000, 2002) used AE to monitor mode I fracture of softwoods (spruce and pine) and hardwoods (alder, oak and ash) and observed that the AE counts up to the maximum force were much higher for the softwoods. Chen et al. (2006) used AE to monitor the failure process of hardwood and softwood test pieces under static and fatigue torsion loading and found it possible to monitor and analyse the failure process in wood by AE techniques. Choi et al. (2007) studied the fracture processes of typical fibre-reinforced-plastic composite laminates with continuous fibre reinforcement. The results showed that the AE characteristics might represent the process of fibre breakage according to the various loading stages, which

expressed characteristic fractures for individual fibre-reinforced composite laminates. The AE hit-event rate, in combination with AE amplitude classifications, could be utilised for non-destructive identification of different fracture mechanisms.

There have been few studies on how to identify the different fracture modes with AE on wood bending. In this work, we studied the AE characteristics in wood during three-point bending test and tried to identify or distinguish different modes of wood fracture. We shall discuss the fracture evolution and mechanisms in relation to the wood microscopic structure with the help of double cantilever beam (DCB) and compression tests.

## MATERIALS AND METHODS

### Test pieces

In order to investigate the AE characteristics of different species in the process of bending, an air-dried softwood (*Picea jezoensis*) and a hardwood (*Castanopsis hystrix*) were used for the test pieces made up of two groups: (1) standard specimens, 300 mm (L) × 20 mm (T) × 20 mm (R) in size (Figure 1a) and (2) notched specimens, 300 mm (L) × 30 mm (T) × 20 mm (R) mm in size, where L, R and T indicate the longitudinal, radial and tangential directions respectively. For the notched specimen, a 10-mm sharp cut, using a razor blade, was made at the tangential direction at the centre of the

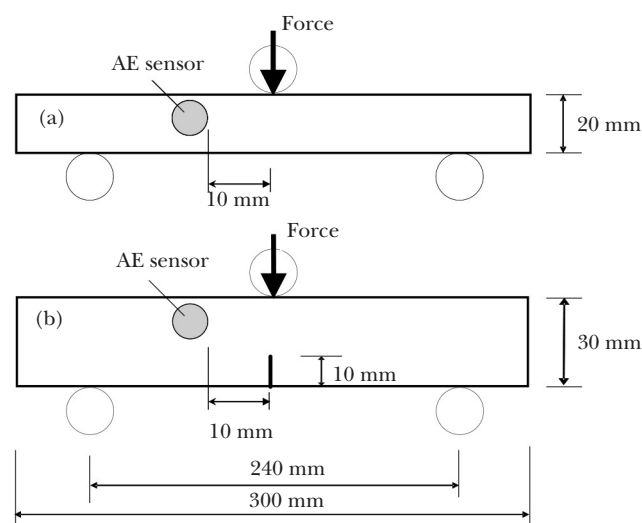


**Figure 1** Three-point bending test and AE sensor location: (a) standard specimen and (b) notched specimen

specimen. Thus the net area was 20 (T) × 20 (R) mm<sup>2</sup> in front of the cut (Figure 1b). *Picea jezoensis* was obtained from a 79-year-old tree (diameter at breast height (dbh) 27.8 cm) in north-east China and *C. hystrix* was obtained from a 122-year-old tree (dbh 56.3 cm) in Jiangxi province, China. The total number of specimens was 120, with 30 specimens per species for each group. The three-point bending test was adopted at tangential direction. The moisture content of the specimens was about 13%.

**Acoustic emission measurement**

The bending tests were performed on the computer-controlled material testing machine. All tests were conducted with controlled loading deflection and similar loading speed. At the same time, the force-deflection curve was drawn automatically by the computer during testing.

AE waves were detected by an AE sensor mounted on the specimen with ethyl α-cyanoacrylate glue. The distance between sensor and middle of the specimen was kept to 10.0 ± 0.1 mm (Figure 1). AE measurement data were recorded using a four-channel AE detection system. Its sampling rate reached 5 million samples per second and the conversion accuracy of the module was 12 bits. Scale range was between ± 10 mV and ± 10 V. The resonant frequency of the AE sensor (R15) was 150 kHz. The preamplifier transmission gain of the AE sensor was 40 dB. The threshold voltage of the AE system was set between 35 and 55 dB depending on test requirements. A band-pass filter of 100–300 kHz eliminated any low frequency emissions: the generated extraneous noise in the laboratory was thus

eliminated and only the frequency range corresponding to optimum sensor efficiency was allowed to pass through. The AE signals of the wood fracture process were then analysed automatically by the AE detection system. All these experiments were conducted at 23 ± 2 °C and relative humidity of about 66 ± 3%.

**RESULTS AND DISCUSSION**

**Acoustic emission characteristics of bending test**

When a wood specimen is loaded at bending test, the load–deflection curve is presented in three stages, i.e. (1) linear elastic deformation stage, (2) non-linear deformation stage and (3) toughness fracture stage. Figures 2a and 3a show this process for the two timber species. Wood fracture is a complex multi-level and multi-stage process. The molecular chain rearrangement, slip, orientation and fracture can be observed under the microscope. During bending, as the wood cracks, the crack will grow and propagate and finally, fracture. All the microscopic and macroscopic material structure changes come along with energy saving and releasing. Therefore, apart from the AE cumulative counts and AE events, peak amplitude A<sub>max</sub>, the event energy and energy rate were determined in this analysis.

**Bending test of standard specimen**

Figures 2–3 show the force vs deflection and AE cumulative counts vs deflection compared with events root mean square (RMS) of voltage

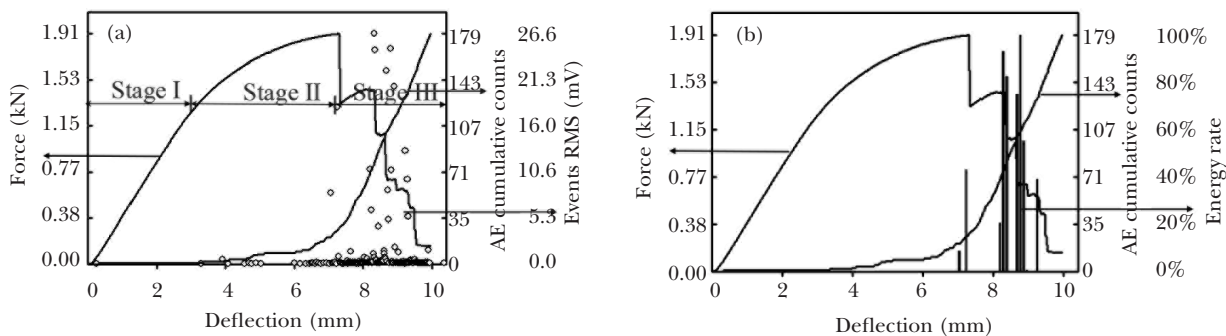


**Figure 2** (a) Force vs deflection and AE cumulative counts vs deflection compared with events RMS vs deflection and (b) force vs deflection and AE cumulative counts vs deflection compared with energy rate vs deflection for *Picea jezoensis* for standard specimen under three-point bending tests; RMS = root mean square, AE = acoustic emission

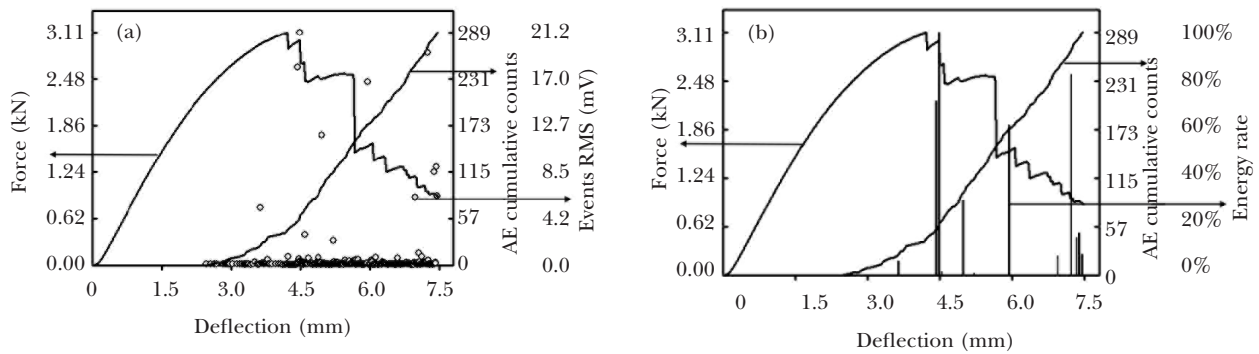


**Figure 3** (a) Force vs deflection and AE cumulative counts vs deflection compared with events RMS vs deflection and (b) force vs deflection and AE cumulative counts vs deflection compared with energy rate vs deflection for *Castanopsis hystrix* for standard specimen under three-point bending test; RMS = root mean square, AE = acoustic emission

vs deflection and the variations of force vs deflection and AE counts vs deflection compared with energy rate vs deflection for *P. jezoensis* and *C. hystrix* for standard specimens under the three-point bending tests. There were no AE counts in the linear elastic deformation stage for standard specimen, i.e. there was no damage and the specimen was unchanged. When it entered into the non-linear deformation stage and because the compressive strength was less than the tensile strength of wood, the compressed area started to yield and as the unaffected (neutral) area reacted to maintain the overall balance (Figure 4), the curve of force vs deflection was non-linear. There was only a small number of AE signals in the early part of this stage (the difference depending on the tree species, the texture orientation and the threshold value because the helically-wound cellulose cell wall reinforcement extends elastically within the matrix of hemicellulose and lignin) and in the second half of the stage, there was rapid increase in AE signals due to the cell interface and interlaminar shear (and layer resulting from the slip and shear within the molecular chain of cellulose). Then it entered into the toughness fracture stage and it emitted a high-energy elastic wave produced by the fibre fracture and pull-out. Usually, the wood beam specimen kept its integrity up to a certain load in the post-fracture period. As the specimen displayed convex bending under the continuous tension, microfracture damage resulted and this damage zone expanded to absorb the energy before a pull-out of the fibre cluster in the fracture in a release of high-energy wave. The interlocking form from the fracture surface in

the tension stress zone was almost flush with the compression stress zone, similar to brittle fracture (Figure 5), which resulted from reduction of the anti-break strength due to the crushing loss of the wood cells in this zone.

### Bending test of notched specimen

Figures 6–7 show variations of force vs deflection and AE cumulative counts vs deflection compared with events RMS vs deflection and curves of force vs deflection and AE cumulative counts vs deflection compared with energy rate vs deflection for *P. jezoensis* and *C. hystrix* for notched specimens under the three-point bending test. A notched wood specimen also presented three stages in the bending failure process. However, a large quantity of low-amplitude low-energy AE was generated when the load increased to about 30–50% of the maximum force  $F_{max}$  (Figures 6a and 7a). At the same time, lateral cracks were found around the crack tip on the surface of the specimen; the force–deflection curve would present a salient point due to the stiffness changes. Figure 8 shows the cell interface and interlaminar shear of lateral cracks for *P. jezoensis*. The lateral cracks expanded parallel to the wood grain in the interlayer and with the increase of load the cracks expanded slowly and eventually stopped. About a 20-mm high new beam section was formed behind the original transverse crack, similar to the standard specimen (Figure 9). The AE characteristics of the notched specimen fracture behaviour were similar to those of the standard specimen. It showed good toughness. There were no significant differences

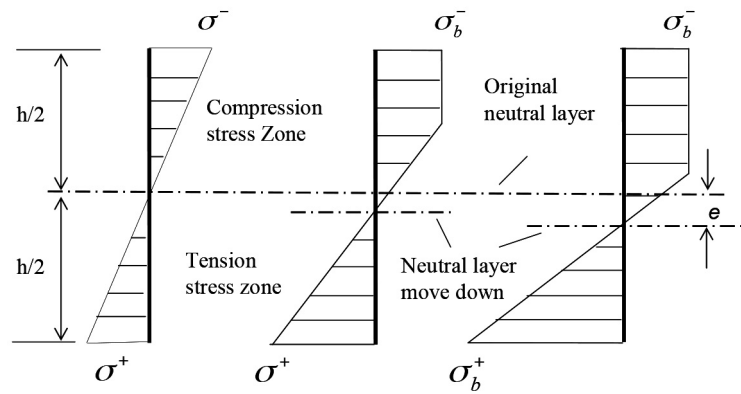


**Figure 4** Sketch of the centre axial of the beam as it was moved and pulled in the bending process

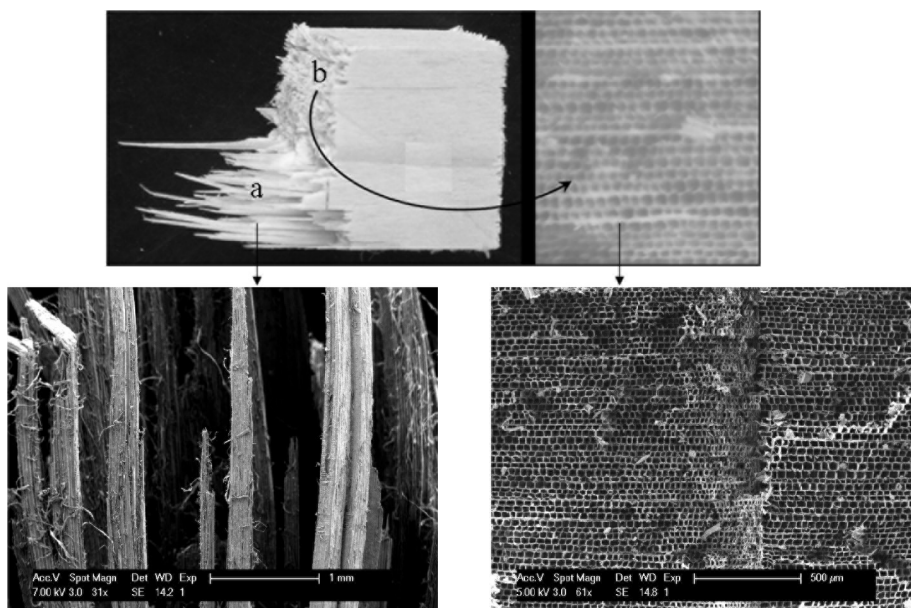


**Figure 5** Scanning electron microscopy observation of the fracture surface of the standard specimen of *Picea jezoensis*: (a) toughness fracture zone and (b) brittle fracture zone

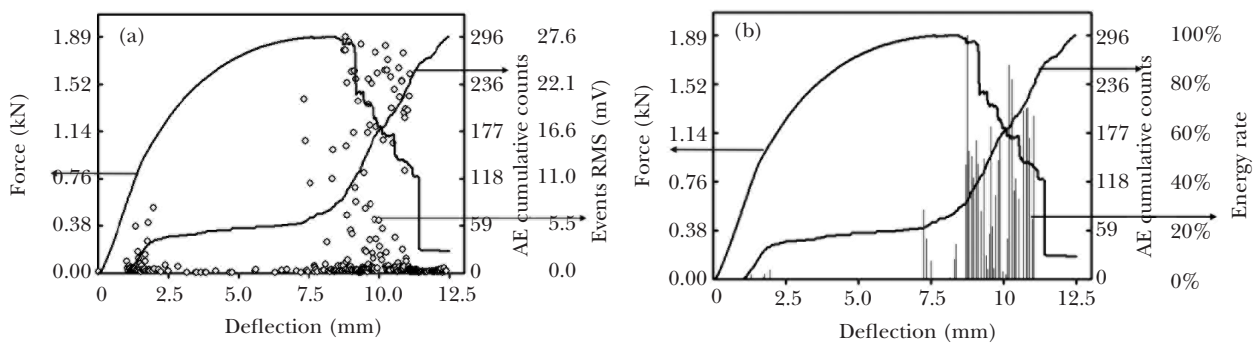


**Figure 6** (a) Force vs deflection and AE cumulative counts vs deflection compared with events RMS vs deflection and (b) force vs deflection and AE cumulative counts vs deflection compared with energy rate vs deflection for *Picea jezoensis* for notched specimen under three-point bending test; RMS = root mean square, AE = acoustic emission

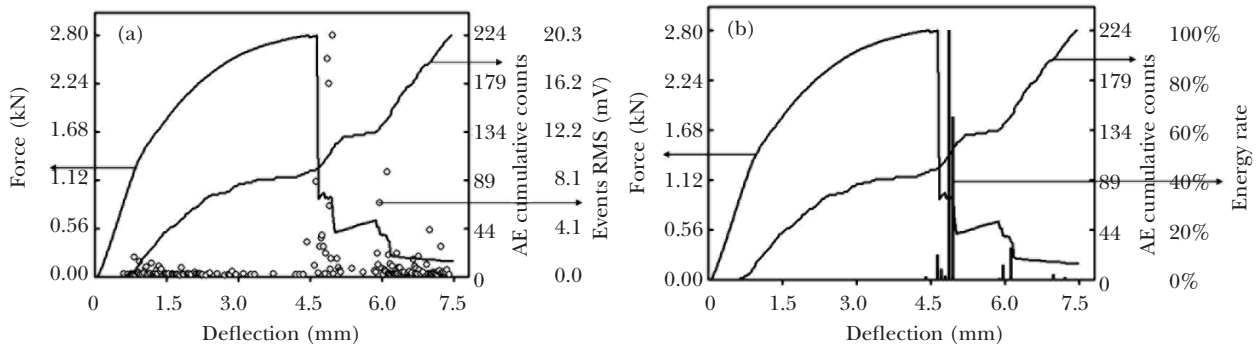


**Figure 7** (a) Force vs deflection and AE cumulative counts vs deflection compared with events RMS vs deflection and (b) force vs deflection and AE cumulative counts vs deflection compared with energy rate vs deflection for *Castanopsis hystrix* for notched specimen under three-point bending test; RMS = root mean square, AE = acoustic emission

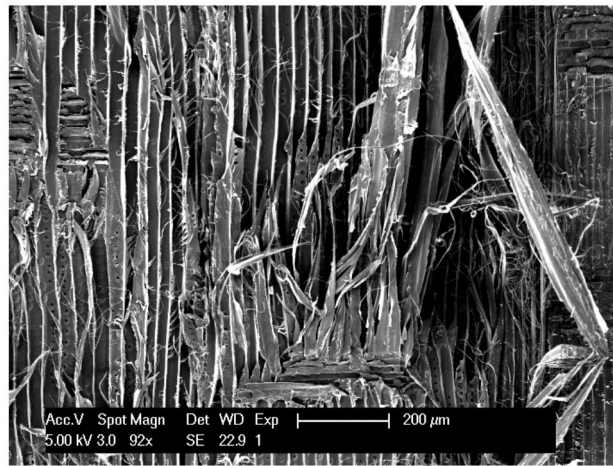


**Figure 8** Scanning electron micrograph of the cell interface and interlaminar shear of lateral cracks for *Picea jezoensis*

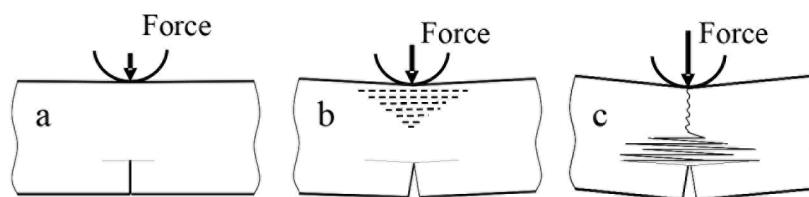


**Figure 9** Sketch of the bending process on a notched specimen: (a) formation of lateral cracks on the crack tip, (b) formation and expansion of the collapsed area and (c) fibre fracture layer by layer of the tensile zone in brittle fracture of the collapsed zone

of the bending strength in the statistical sense between the standard specimen and the notched specimen after deducting the prefabricated sharp crack (Table 1), which once again showed that specimen containing crack perpendicular to the wood grain would not produce low stress rupture because of the crack tip stress singularity.

**Analysis of AE characteristics and source**

There is relationship between AE signal wave characteristics and AE source (damage models). The experiments showed there were four kinds of typical damage models applied to the specimens with cracks made perpendicular to the grain in

**Table 1** Bending strength values of the standard and notched specimens

Species	Sample type	Number of samples	Average (MPa)	SD	CV
<i>Picea jezoensis</i>	Standard specimen	22	74.95	11.06	14.76
	Notched specimen	22	78.23	9.62	12.3
<i>Castanopsis hystrix</i>	Standard specimen	16	122.97	13.26	10.78
	Notched specimen	16	118.08	10.88	9.21

SD = standard deviation, CV = coefficient of variation

the course of the transverse bending process, i.e. cell-wall damage and spallation, cell-wall buckling and collapse, formation and expansion of the microfracture damage area, and cell-wall fracture. Figure 10 shows the typical time-domain curve of interlaminar fracture and transverse fracture of notched specimen for *P. jezoensis* and combined with Figures 6a and 7a, the characteristics of AE signal in different damage and fracture models are summarised as follows:

- (1) The characteristics of AE signal for the interlaminar fracture stage (i.e. cell-wall damage evolution and spallation) are low amplitude, short duration, low-count and low energy;
- (2) The AE amplitude of wood-cell compressive yields stage (i.e. cell-wall buckling and collapse) is lower or shows lower energy. The signal usually does not count when the signal of the probe is of lower threshold value because of the attenuation of AE wave propagation;
- (3) The AE signal of the wood macroscopic fracture stage (i.e. fibre bundle fracture and pull-out) is of high amplitude, long duration, high-energy and high AE counts;
- (4) The AE signal characteristic with the correspondence of the formation and expansion of the microfracture damage area is more complicated and is the prelude to damage fracture and also exists in the whole period. What makes it different from interlaminar fracture is that the former mainly occurs in type I or peeling and cracking of the cell or cell layer, while the latter is due to the whole material damage by formation, expansion and connection of the microfracture caused by the cell-wall tear or rupture. The AE characteristic, which lies between interlaminar fracture and transverse

fracture, is affected by the relative density, cell-wall thickness, microscopic structure and degree of damage.

Although we have the above understanding, it is still very difficult to distinguish AE signals from different damage models in the bending process. As wood is a multi-level cell structured biological material, there is always a variety of deformation and damage that can change the energy system at the same stage near the zone of the crack tip. Therefore, a DCB experiment along the grain in the wood crack and a compression experiment along the longitudinal and transverse directions were carried out (Figure 11). The DCB test would produce Mode I interlaminar fracture and the compression test would give rise to cell-wall buckling and collapse damage.

The results confirmed the presence of only low amplitude and low energy AE events in the Mode I interlaminar fracture and lower AE signal energy in the compression test. The results conform to the findings of Schniewind et al. (1996).

Based on a large number of AE signal analyses of the damage modes of different tree species with the AE sensor set in the damage source in the 10-cm range, we found that both the maximum of high amplitude AE events voltage,  $V_{\max}$ , and RMS value could be distinguished from different damage modes; the RMS value especially was the most effective. RMS value was directly related to the energy release of the AE events. The  $V_{\max}$  and RMS values corresponding to different damage modes are listed in Table 2.

### Felicity effect

The energy release is irreversible in the process of material damage. It is the same with AE,

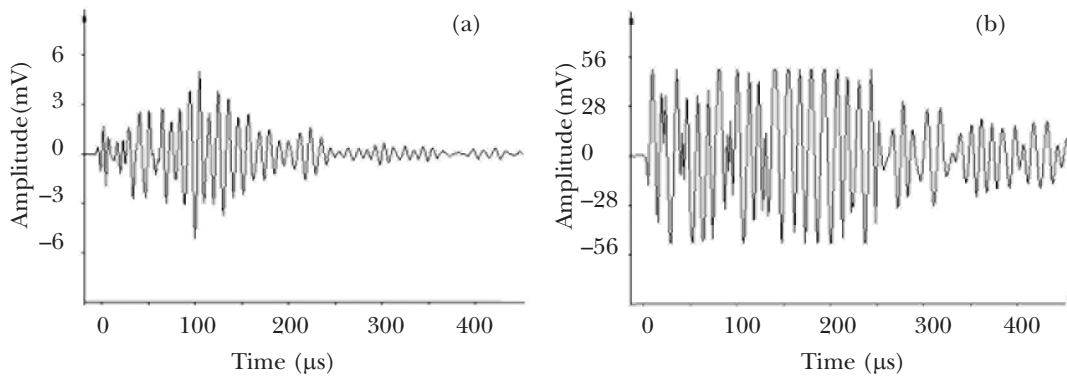


**Figure 10** Time-domain curves of different damage models: (a) interlaminar fracture and (b) cell-wall fracture

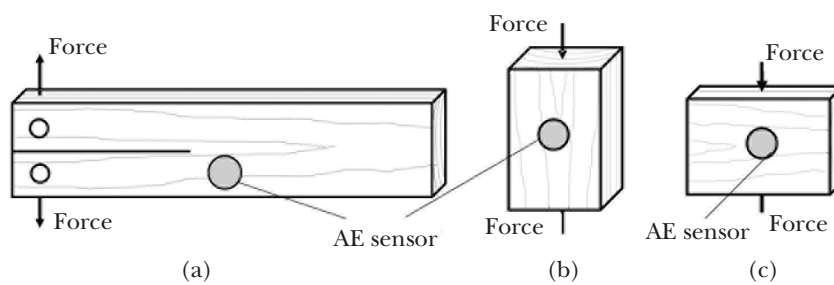


**Figure 11** Sketch of (a) double cantilever beam and (b, c) compression tests; AE = acoustic emission

**Table 2** AE characteristics corresponding to damage modes

Damage mode	$V_{max}$		RMS	
	mV	dB	mV	dB
Cell-wall collapse	< 2	< 65	< 0.4	< 52
Interlaminar fracture	< 10	< 80	< 1.0	< 60
Cell-wall laniate and cracks formation	< 35	< 90	< 10	< 80
Fibre bundle fracture and pull-out	> 35	> 90	> 10	> 80

RMS = root mean square, AE = acoustic emission

which is known as the Kaiser effect. Felicity effect refers to the phenomenon that AE appears when reloading is lower than the previous loading. As a quantitative parameter, it can better reflect the extent of the original material damage or the structure deficiencies. The smaller the Felicity ratio, the more serious is the damage or structure deficiencies. A Felicity ratio of more than 1 means there exists the Kaiser effect; on the other hand, the Felicity effect takes over when the Felicity ratio is less than 1.

Figure 12 shows the course of the cyclic load bending test and the AE analysis of notched

specimen of *P. jezoensis*. There were eight cycles of loading and unloading in the whole test. The first loading and unloading occurred at the beginning of the interlaminar fracture when the Felicity ratio was 0.99, which meant that there existed instability of the structure defect.

The Felicity ratio was more than 1 in the second to sixth loading and unloading because of the stress redistribution of specimens as the lateral crack expanded and gradually stabilised, but there was a declining trend close to the maximum load. The seventh loading and unloading occurred near the maximum load

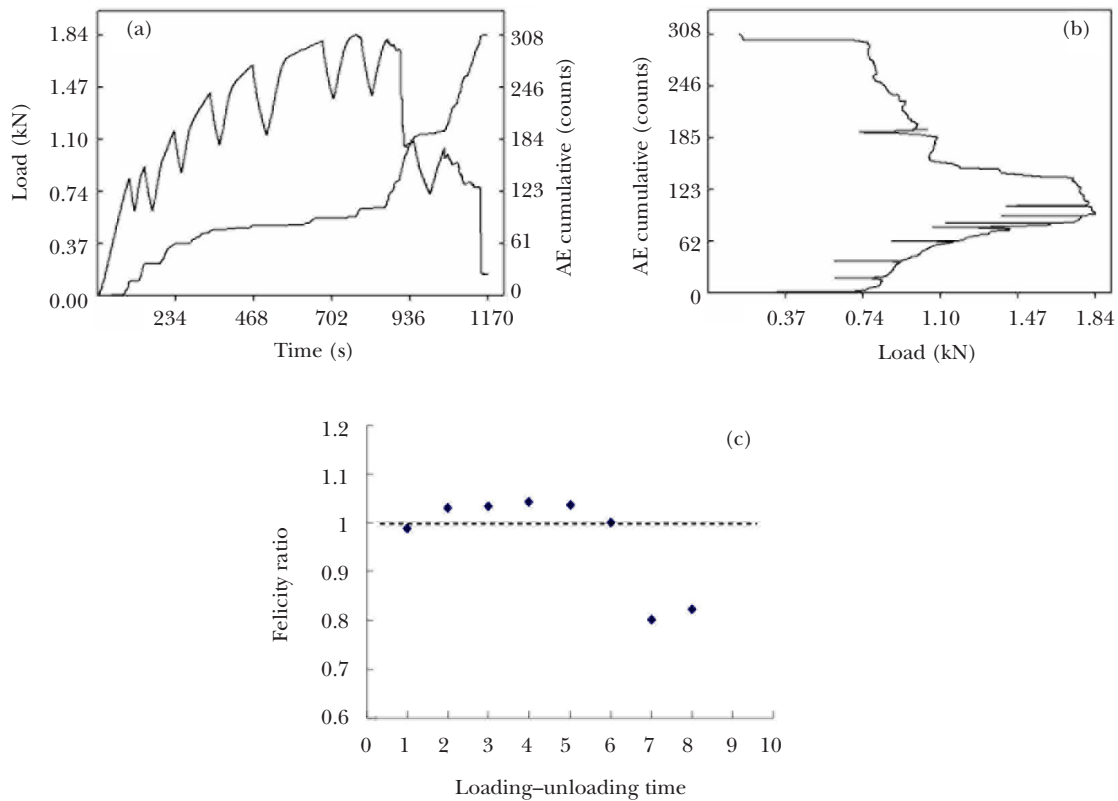


**Figure 12** Cyclic load bending test and analysis of notched specimen of *Picea jezoensis*: (a) load vs time and AE cumulative counts vs time, (b) AE cumulative counts vs load and (c) Felicity ratio vs loading–unloading time; AE = acoustic emission

and the eighth loading and unloading occurred in the third stage of toughness fracture which meant that the material structure suffered serious damage. The repeated load test behaviour of the standard specimen was almost similar to that of the notched specimen. However, the Felicity ratio was more than 1 when the load approached the maximum load in the whole process. Therefore, the bending test of wood in low load, or most of stage II, showed that the Kaiser effect and the high load or toughness fracture stage presented the Felicity effect. As a result, AE technology could better monitor wood damage in practical application.

It needs to be clear that the Felicity phenomenon is different for different wood species and threshold voltages. AE signals could also be produced due to the friction of the microcracks in the process of loading–unloading; so in order to preclude the interference of false damage, the threshold voltage should be set higher than normal. In the loading–unloading of this experiment the threshold voltage was set at 0.39 mV (about 52 dB).

## CONCLUSIONS

A series of AE signals were produced due to the energy release which was caused by the different damage and fracture mechanisms of wood during the bending test. AE technology can help us identify the initiation and expansion of different types of damage of wood components during the loading process. The results showed that AE event counts developed slowly with most being the low amplitude AE events at the low strains and a large number of high amplitude AE events appearing in peak load or fracture stage for standard specimen. The initiation and expansion of crack tip could be monitored efficiently by the AE technique in the whole process of the three-point bending test for the notched wood specimen. The AE signals were related to different damage patterns/modes. The AE characteristics of cell-wall fracture were high amplitude, high energy and long-duration AE events but the AE characteristics of cell-wall damage and spallation, cell-wall buckling and collapse were

low amplitude, low energy and short-duration AE events. The Kaiser effect appeared at low loading and the Felicity effect at high loading under repeated wood bending loading. The Felicity ratio could better indicate the degree of damage of the wood structure. Thus, the behaviour of wood bending fracture could be monitored through non-destructive evaluation using the AE technique.

## ACKNOWLEDGEMENT

This study was supported by the National Natural Science Foundation of China (No. 11072001).

## REFERENCES

- AICHER S, HÖFFLIN L & DILL-LANGER G. 2001. Damage evolution and acoustic emission of wood at tension perpendicular to fiber. *Holz als Roh- und Werkstoff* 59: 104–116.
- BAKUCKAS JG, PROSSER WS & JOHNSON WS. 1994. Monitoring damage growth in titanium matrix composites using acoustic emission. *Journal of Composite Materials* 28: 305–328.
- BOOKER JD. 1994a. Acoustic emission and surface checking in *Eucalyptus regnans* boards during drying. *Holz als Roh- und Werkstoff* 52: 383–388.
- BOOKER JD. 1994b. Acoustic emission related to instantaneous strain in Tasmanian eucalypt timber during seasoning. *Wood Science and Technology* 28: 249–259.
- BUCUR V. 1995. *Acoustics of Wood*. CRC Press, Boca Raton.
- CHEN Z, GABBITAS B & HUNT D. 2006. Monitoring the fracture of wood in torsion using acoustic emission. *Journal of Materials Science* 41: 3645–3655.
- CHOI NS, WOO SC & RHEE KY. 2007. Effects of fiber orientation on the acoustic emission and fracture characteristics of composite laminates. *Journal of Materials Science* 42: 1162–1168.
- DILL-LANGER G & AICHER S. 2000. Monitoring of microfracture by microscopy and acoustic emission. Pp 93–104 in *Proceedings International Conference on Wood and Wood Fiber Composites*. 28 May 2000, Stuttgart.
- KAISER J. 1950. An investigation into the occurrence of noises in tensile tests or a study of acoustic phenomena in tensile tests. PhD thesis, Technische Hochschule, Munich.
- KATSAGA T ET AL. 2007. Acoustic emission imaging of shear failure in large reinforced concrete structures. *International Journal of Fracture* 148: 29–45.
- NOGUCHI M ET AL. 1987. Feedback control for drying *Zelkova serrata* using in-process acoustic emission monitoring. *Forest Products Journal* 37: 28–34.
- ONO K, JENG JS & YANG JM. 1991. Fracture mechanism studies of a carbon fiber-PEEK composite by acoustic emission. Pp 395–404 in Sachse W, Roget J & Yamaguchi K (eds) *Acoustic Emission: Current Practice and Future Directions*. American Society for Testing and Materials, Philadelphia.
- QUARLES SL. 1992. Acoustic emission associated with oak during drying. *Wood and Fiber Science* 24: 2–12.
- REITER A, STANZL-TSCHEGG SE & TSCHEGG EK. 2000. Mode I fracture and acoustic emission of softwood and hardwood. *Wood Science and Technology* 34: 417–430.
- REITER A, STANZL-TSCHEGG SE & TSCHEGG EK. 2002. Fracture characteristics of different wood species under Mode I loading perpendicular to the grain. *Materials Science and Engineering A* 332: 29–36.
- SCHNIEWIND AP, QUARLES SL & LEE H. 1996. Wood fracture, acoustic emission, and the drying process Part 1. Acoustic emission associated with fracture. *Wood Science and Technology* 30: 273–281.